

## Modelling and estimating trajectory points from RTK-GNSS based on an integrated modelling approach

Ravenny Sandin Nahar<sup>1</sup>, Kok Mun Ng<sup>1,2</sup>, Fadhlan Hafizhelmi Kamaruzaman<sup>1,2</sup>,  
Noorfadzli Abdul Razak<sup>1</sup>, Juliana Johari<sup>1</sup>

<sup>1</sup>School of Electrical Engineering, College of Engineering, Universiti Teknologi MARA, Shah Alam, Malaysia

<sup>2</sup>Vehicles Intelligence and Telematics Lab, School of Electrical Engineering, College of Engineering, Universiti Teknologi MARA, Shah Alam, Malaysia

### Article Info

#### Article history:

Received Aug 3, 2023

Revised Dec 7, 2023

Accepted Jan 12, 2024

#### Keywords:

ARIMA errors  
Gaussian process  
Integrated model  
Linear regression  
RTK-GNSS

### ABSTRACT

The sparse Gaussian process regression (GPR) has been used to model trajectory data from Real time kinematics-global navigation satellite system (RTK-GNSS). However, upon scrutinizing the model residuals; the sparse GPR model poorly fits the data and exhibits presence of correlated noise. This work attempts to address these issues by proposing an integrated modeling approach called GPR-LR-ARIMA where the sparse GPR was integrated with the linear regression with autoregressive integrated moving average errors (LR-ARIMA) to further enhance the description of the trajectory data. In this integrated approach, the predicted trajectory points from the GPR were further described by the LR-ARIMA. Simulation of the GPR-LR-ARIMA on three sets of trajectory data indicated better model fit, revealed in the normally distributed model residuals and symmetrically distributed scatter plots. Correlated noise was also successfully eliminated by the model. The GPR-LR-ARIMA outperformed both the GPR and LR-ARIMA by its ability to improve mean-absolute-error in 2-dimension positioning by up to 86%. The GPR-LR-ARIMA contributes to enhancement of positioning accuracy of dynamic GNSS measurements in localization and navigation system with good model fit.

This is an open access article under the [CC BY-SA](https://creativecommons.org/licenses/by-sa/4.0/) license.



### Corresponding Author:

Kok Mun Ng

School of Electrical Engineering, College of Engineering, Universiti Teknologi MARA

40450 Shah Alam, Selangor, Malaysia

Email: ngkokmun@uitm.edu.my

## 1. INTRODUCTION

Global navigation satellite system (GNSS) comprised of a group of satellites that generate and transmit positioning, timing, and navigation data from space to connected receivers or devices on earth. GNSSs were used in various applications such as locating potential forest fires [1]; space surveillance and tracking system [2]; observation of coastal tides [3]; cadastral surveying [4] and localization and navigation system [5]. In addition to GNSS, simultaneous localization and mapping systems (SLAM) [6]-[8] and indoor localization and navigation systems [9]-[10] were developed for localization and navigation systems.

GNSS positioning accuracy in localization and navigation systems could be affected by signal interference [11] and the absence of satellite signals when navigating under tree canopy, tunnels or in-between buildings [12]. Real-time kinematic global navigation satellite systems (RTK-GNSS) could enhance the positioning accuracy; however, it was reported that the accuracy of positioning was affected by the quality of the receiver and satellite position when the receiver moves in different landscapes [13]-[16]. For

example, performance evaluation conducted on low-cost RTK-GNSSs tested in different landscapes did not achieve fixed-integer solution for long duration of time in dynamic applications [16].

To improve the positioning accuracy of localization and navigation systems, Gaussian process regression (GPR) has been used to model odometry errors in SLAM [7] and inertial measurement system errors in [12]. GPR is a type of machine learning that is non-parametric and adopts a Bayesian regression approach. The GPR model is well suited for data that is correlated, possesses time-varying covariates, nonlinear and non-stationary [17]. The trained GPR model could be used for processing position errors from GNSS in static and dynamic measurements.

Some works applied the GPR to model measurement errors from static GNSS stations resulted in prediction of improved positions with better accuracy [18], [19]. On the other hand, Kortessalmi *et al.* [20] performed coarse approximation of GNSS measurements in dynamic applications to model and estimate position variance in bus trajectory using the GPR. Xue-mei *et al.* [21] developed GPR models to predict the trajectories of incoming vehicles at a traffic intersection using lateral and vertical position information from vision sensors. Yoon *et al.* [22] utilized GPR, assisted by a path-following model, to predict the future state of a cut-in vehicle. Research on such dynamic modeling of trajectory contributes to better positioning accuracy in navigation systems. However, current research did not scrutinize the performance of the GPR model fit on the trajectory dynamic data [20]-[26].

It is essential to further scrutinize the GP models' residuals for un-modeled errors that directly reflect the model performance. These un-modeled errors are variations in the residuals of a mathematical model, which are challenging to be further modelled by incorporating additional parameters [27]. This gap was bridged by Nahar *et al.* [28] where predictions of dynamic measurements from RTK-GNSS using the sparse GP (a type of GPR) was further scrutinized and studied. Although, the sparse GP could predict dynamic trajectory points with better accuracy; the residuals of the models revealed poor model fit [28]. Therefore, there is a need to ensure good model fit when using GPR to model and predict dynamic GNSS points. Methods such as reweighing and retraining of GP models [18] using weighted least square [29] and fitting an appropriate noise model [19] have been implemented to improve fitness of models describing data of static GNSS stations. However, these methods were tedious and computationally expensive; hence, may not be feasible to optimize model fit in dynamic data.

This paper revisits the modeling of dynamic trajectory data using sparse GPR method introduced by Nahar *et al.* [28]. The aim of this work is to improve model fitting and positioning accuracy of dynamic trajectory data described by the sparse GPR models [28]. We proposed an integrated model approach using both sparse GPR and Linear regression with autoregressive moving average errors (LR-ARIMA) models that were developed by Nahar *et al.* [28] and Ng *et al.* [30] respectively to describe dynamic trajectory data. ARIMA error models could further describe the un-modelled errors in the residuals of the GPR with better correlation in the model based on time series method [30]-[34]. The predicted outputs from the sparse GPR are fed into the LR-ARIMA, forming an integrated two-stage model named as GPR-LR-ARIMA. The performance of the predictions from the GPR-LR-ARIMA were compared with sparse GPR to demonstrate improvement in model fit. Positioning accuracy produced by the sparse GPR, LR-ARIMA and GPR-LR-ARIMA were compared to reveal the advantage of this model integration. The method contributes to enhancement of positioning accuracy of dynamic GNSS measurements in localization and navigation system with improved model fit. Section 2 of this paper outlines the method that includes data sets used in section 2.1 whereas section 2.2 outlines the model integration method. Section 3 presents the results and evaluates the model performance.

## 2. METHOD

### 2.1. Data sets

Three sets of trajectory data were employed from [28]. The trajectory data was collected using EMLID Reach RTK-GNSS in the location shown in Figure 1, which is situated in the city of Shah Alam, Malaysia [35]. It comprised of a base station (marked "X") which was placed in the football field to project carrier phase corrections to the rover with baseline ranging from 200 to 500 meters. The rover moved along the trajectory (the red path) that encircles residential houses, buildings, structures and trees. The trajectory was affected by multipath effects as the direct line of sight between the rover and base station was obstructed by building and structures. Data was logged by connecting the rover to the laptop via serial communication. A MATLAB program was developed to read National Marine Electronics Association (NMEA) \$GPGAA-format from the rover and log all geodetic coordinates and fix quality indicators. The sampling rate is set at 0.5 Hz. The data has been cleaned to remove outliers and flawed data by removing the spiked data points in each of data set. Spiked data points were logged measurements that deviated more than 5 meters from the trajectory, which can be visually observed using Google Earth. All data logging and computing were performed using MATLAB R2017b on a laptop running on an Intel Core i5 processor.



$$y_t = \beta x_t + c + \mu_t$$

$$(1 - \alpha_1 L - \dots - \alpha_p L^p)(1 - L)^D \mu_t = (1 + \phi_1 L + \dots + \phi_q L^q) \varepsilon_t \tag{1}$$

In step 5, a linear regression relationship  $X = \beta X_{GPR} + c$  between predicted  $X_{GPR}$  points from the sparse GPR with the  $X_{east}$  ground truth is obtained from each data set. Linear regression model,  $Y = \beta Y_{GPR} + c$  is also established for predicted  $y_{GPR}$  points from the sparse GPR with the  $Y_{north}$  ground truth. Subsequently, the autocorrelation function (ACF) and partial correlation function (PACF) plots are applied on the residuals of the linear regression model to estimate the ARIMA error models for each trajectory in step 6. This estimation draws on the unique relationship of ACF and PACF plots explained in [34].

In step 7, the Akaike Information Criterion (AIC) is used to identify the best fitted ARIMA error model for both x and y axes respectively. The lowest AIC is used to identify the type of ARIMA error. Based on (1), LR-ARIMA models are developed for x-axis coordinates and y-axis coordinates as shown in (2) and (3) respectively. The  $X_{opt}$  and  $Y_{opt}$  in (2) and (3) respectively depict the final optimized coordinates produced by GPR-LR-ARIMA model.

$$X_{opt} = \beta X_{GPR} + c + \mu_t$$

$$(1 - \alpha_1 L - \dots - \alpha_p L^p)(1 - L)^D \mu_t = (1 + \phi_1 L + \dots + \phi_q L^q) \varepsilon_t \tag{2}$$

$$Y_{opt} = \beta Y_{GPR} + c + \mu_t$$

$$(1 - \alpha_1 L - \dots - \alpha_p L^p)(1 - L)^D \mu_t = (1 + \phi_1 L + \dots + \phi_q L^q) \varepsilon_t \tag{3}$$

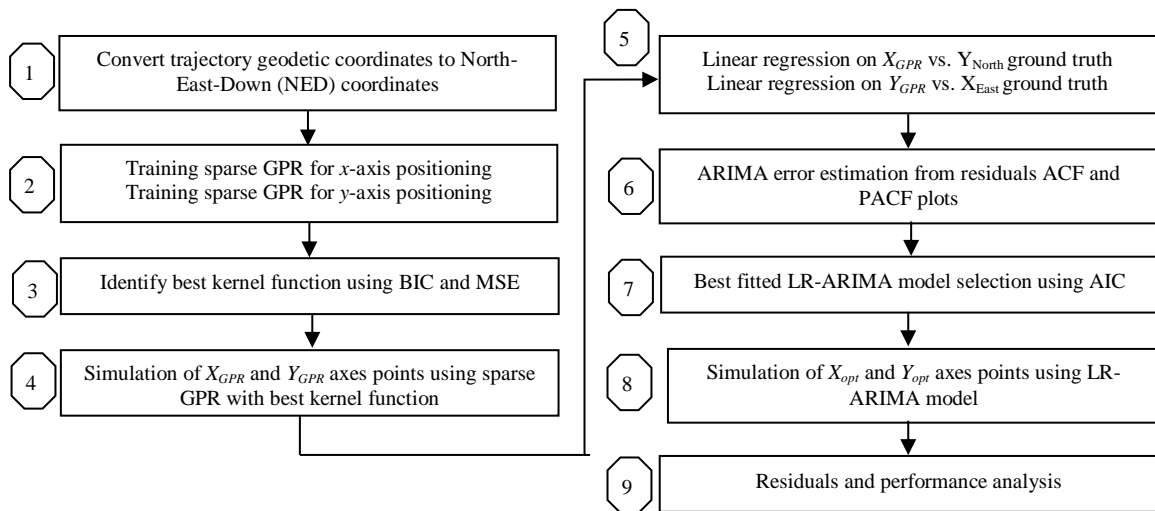


Figure 2. GPR-LR-ARIMA integrated model

In step 8, the best fitted LR-ARIMA models are implemented to simulate  $X_{opt}$  and  $Y_{opt}$ , which are the final outputs from the GPR-LR-ARIMA. In step 9, residuals analysis is conducted on the sparse GPR and GPR-LR-ARIMA models to compare the model fitness. The mean absolute error (MAE) and root mean square error (RMSE) in 2-dimensional position (2D) on original data, predictions from the sparse GPR, LR-ARIMA and GPR-LR-ARIMA models are compared to evaluate their performance in producing coordinate points with improved accuracy.

### 3. RESULTS AND DISCUSSION

#### 3.1. Results of integrated model

The sparse GPR models based on FIC approximation method was trained for x-axis using 250 inducing points from a total of 833 logged x coordinate points in each of the three data sets [28]. This was repeated for the y-axis using y coordinate points. The EXP, Squared SQEXP, Matern 3/2 (MAT32), Matern 5/2 (MAT52) and Rational Quadratic (RATQUA) kernel functions were evaluated respectively.

For brevity, Table 1 summarized the best performed kernel functions for data set 1, 2 and 3 respectively in [28]. The best kernel function for each axis was identified during model validation by identifying the lowest BIC value and lowest MSE (produced by the 10-fold cross validation). The row labelled MSE-X summarized the lowest MSE of the respective sparse GPR model trained for x-axis positioning, whereas MSE-Y shows the lowest MSE of the respective sparse GPR model for y-axis positioning of each data set. BIC-X and BIC-Y are respectively lowest BIC values for x-axis and y-axis GPR models of each of the data set. The best kernel for each axis is also shown in Table 1. The SQEXP and MAT52 outperformed the other kernel functions by producing the lowest BIC and AIC, indicating the optimal model fit.

The sparse GPR models with the best performing kernel were applied in each data set to predict  $X_{GPR}$  and  $Y_{GPR}$  points. Subsequently, linear regression (LR) models were developed to established  $X = \beta X_{GPR} + c$  and  $Y = \beta Y_{GPR} + c$  respectively. Table 2 summarized the established LR models when the respective  $X_{GPR}$  and  $Y_{GPR}$  predicted from each data set were linearly regressed with the ground truth data.

Table 1. Best performed kernel functions

	Data Set 1	Data Set 2	Data Set 3
MSE-X	0.0483	0.0991	0.0768
MSE-Y	0.1196	0.2414	0.0890
BIC-X	2940.00	2950.00	2940.00
BIC-Y	2200.00	2270.00	2200.00
Best kernel for x-axis	SQEXP	SQEXP	SQEXP
Best kernel for y-axis	MAT52	SQEXP	MAT52

Table 2. Linear regression models

Data set	$X_{East}$		$Y_{North}$	
	Regression model	$R^2$	Regression model	$R^2$
1	$X = 0.999X_{GPR} + 0.238$	0.9776	$Y = 0.998Y_{GPR} + 0.103$	0.9788
2	$X = 1.000X_{GPR} + 0.224$	0.9776	$Y = 0.999Y_{GPR} + 0.176$	0.9762
3	$X = 1.000X_{GPR} - 0.097$	0.9821	$Y = 0.999Y_{GPR} + 0.063$	0.9768

According to the method in step 6 (Figure 2), the residuals from these LR models were further analyzed using the ACF and PACF relations in [34] to estimate all possible ARIMA errors. The ACF and PACF relations analysis was conducted after first order differencing on the non-stationary model residuals. As an example, Figure 3 shows ACF and PACF plots of the differenced LR model residuals for x and y axes of data set 2. The integrated moving average (IMA) or autoregressive integrated (ARI) models can be the possible error models as the ACF and PACF displays cut-off at the lag axis for both x-axis (See Figures 3(a) and 3(b)) and y-axis (See Figures 3(c) and(d)).

Based on PACF and ACF relations of the axis residuals, possible ARI, IMA or ARIMA models were listed in Table 3. The data sets possibly possessed ARI and IMA errors. However, ARIMA errors were not observed in any of the data sets.

In step 7 (Figure 2), an algorithm written in MATLAB calculates the AIC values of the model errors and identify the best IMA and ARI order for each data set axis respectively. The results in Table 4 shows the best IMA, and ARI order identified based on the lowest value of AIC (i.e. font in bold) in each data set. Based on the lowest AIC values; data set 1 is best modelled with ARI (4, 1, 0) for x-axis and ARI (3, 1, 0) for y-axis. ARI (8, 1, 0) and IMA (0, 1, 1) are best fitted errors for data set 2, whereas data set 3 is best modelled with ARI (4, 1, 0) and ARI (2, 1, 0) for each axes respectively. All estimated ARI and IMA models concurred with all the assumed models listed in Table 3.

Table 5 shows the fitted LR-ARIMA models estimated for each data set using the ARI and IMA order in Table 4. All LR-ARIMA model estimation were done using the MATLAB Linear Regression with ARIMA toolbox. The linear regression model with their respective autoregressive (AR) and moving average (MA) coefficients were estimated respectively for each data set. For example, the LR-ARIMA model estimated from MATLAB for data set 1 possessed only AR coefficients up to the 4th order (i.e. 0.646, 0.288, 0.197 and 0.098) for x-axis and 3rd order (i.e. 0.357, 0.134 and 0.994) for y-axis positioning. Only data set 2 possessed moving average errors to the first order with a coefficient of 0.340.

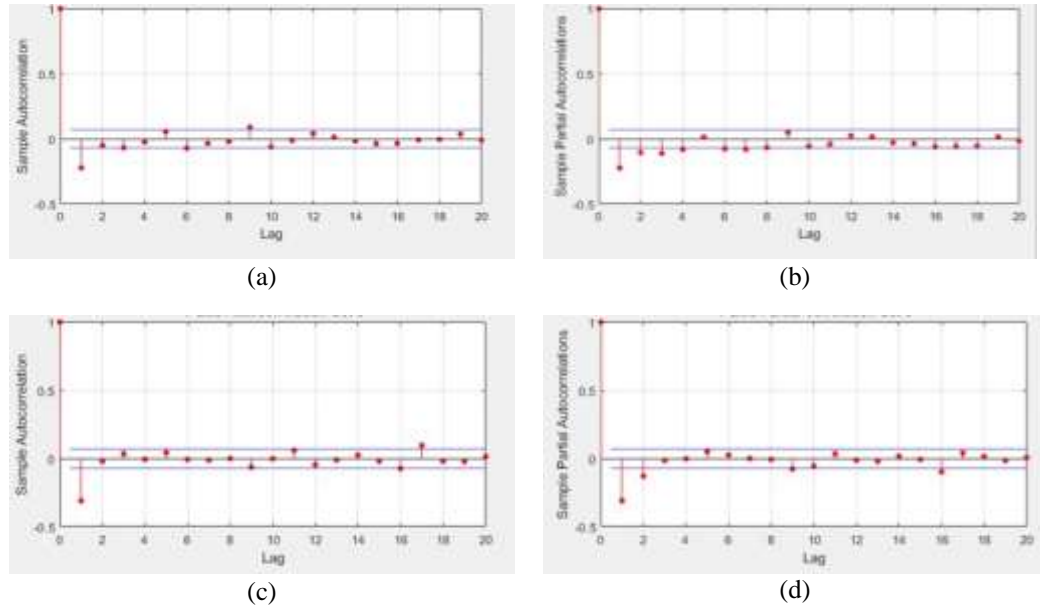


Figure 3. Residuals analysis of LR model of data set 2: (a) ACF of x-axis residuals, (b) PACF of x-axis residuals, (c) ACF of y-axis residuals, and (d) PACF of y-axis residuals

Table 3. Possible ARI, IMA or ARIMA error models for x-axis and y-axis based on ACF and PACF relations

Data Set	x-axis Residuals			y-axis Residuals		
	ACF Characteristics	PACF Characteristics	Possible Model	ACF Characteristics	PACF Characteristics	Possible Model
1	Die out	Cut off	ARI	Die out	Cut off	ARI
2	Cut off	Cut off	ARI or IMA	Cut off	Cut off	ARI or IMA
3	Cut off	Cut off	ARI or IMA	Die out	Cut off	ARI

Table 4. ARI and IMA error models for x-axis and y-axis

Model			Data Set		
			1	2	3
$X_{east}$ Error Models	ARI	Order	<b>4,1,0</b>	<b>8,1,0</b>	<b>4,1,0</b>
		AIC	<b>-1163.79</b>	<b>-584.99</b>	<b>-911.90</b>
	IMA	Order	0,1,2	0,1,2	0,1,1
		AIC	-1161.38	-578.52	-910.73
$Y_{north}$ Error Models	ARI	Order	<b>3,1,0</b>	2,1,0	<b>2,1,0</b>
		AIC	<b>-1170.41</b>	-532.08	<b>-1095.32</b>
	IMA	Order	0,1,1	<b>0,1,1</b>	0,1,2
		AIC	-1162.66	<b>-532.54</b>	-1091.40

Table 5. Fitted LR-ARIMA models for x and y axes

Data set	$X_{east}$	$Y_{north}$
1	$X_{opt} = 0.999X_{GPR} + 0.238 + \mu_t$ $(1 + 0.646L + 0.288L^2 + 0.197L^3 + 0.098L^4)(1 - L)\mu_t = \varepsilon_t$	$Y_{opt} = 0.998Y_{GPR} + 0.103 + \mu_t$ $(1 + 0.357L + 0.134L^2 + 0.994L^3)(1 - L)\mu_t = \varepsilon_t$
2	$X_{opt} = 1.000X_{GPR} + 0.224 + \mu_t$ $(1 + 0.277L + 0.155L^2 + 0.148L^3 + 0.105L^4 + 0.027L^5 + 0.108L^6 + 0.098L^7 + 0.067L^8)(1 - L)\mu_t = \varepsilon_t$	$Y_{opt} = 1.000Y_{GPR} + 0.176 + \mu_t$ $(1 - L)\mu_t = (1 - 0.340L)\varepsilon_t$
3	$X_{opt} = 1.000X_{GPR} - 0.097 + \mu_t$ $(1 + 0.620L + 0.361L^2 + 0.138L^3 + 0.068L^4)(1 - L)\mu_t = \varepsilon_t$	$Y_{opt} = 0.999Y_{GPR} + 0.063 + \mu_t$ $(1 + 0.547L + 0.220L^2)(1 - L)\mu_t = \varepsilon_t$

### 3.2. Performance evaluation

The LR-ARIMA models in Table 5 were used to simulate  $X_{opt}$  and  $Y_{opt}$  from the simulated  $X_{GPR}$  and  $Y_{GPR}$  data sets. To illustrate performance of model fit; the ACF, histogram and QQ-Plot of the model residuals from data set 2 are used to compare model fitness of sparse GPR and GPR-LR-ARIMA as shown in

Figures 4 and 5. The ACF of x-axis residuals in Figure 4(a) and the ACF of y-axis residuals in Figure 5(a) of the GPR model for data set 2 show the data were correlated, indicating the presence of correlated noise. On the other hand, the ACF of x-axis and y-axis residuals of the GPR-LR-ARIMA in Figure 4(b) and 5(b) respectively indicated non-correlated residuals. Hence, the correlated noise which appears in the GPR models was eliminated by the GPR-LR-ARIMA integrated model. The normally distributed histograms and QQ-Plots for both x and y axis residuals of the GPR-LR-ARIMA model indicated good model fit (see Figure 4(b) and 5(b) respectively). In addition, the scatter plot of the GPR-LR-ARIMA residuals versus fitted values for both axes shown in Figure 6, displayed points that were symmetrically distributed and clustering towards the zero mean. In contrast, the GPR model displayed kurtosis behavior in the histograms and QQ-Plots for both axes (see Figure 4(a) and 5(a)) indicating poor model fitting. This behavior was also observed in the histogram and QQ-plots of data set 1 and 3. For brevity, their results are not shown here.

Table 6 presents the MAEs and RMSEs of 2D position errors achieved by the GPR, LR-ARIMA and GPR-LR-ARIMA models respectively compared to the original data performance. The GPR-LR-ARIMA models were observed to perform the best in terms of MAE and RMSE for all three data sets when compared to the GPR and LR-ARIMA. As shown in Figure 7, the GPR-LR-ARIMA improved the position errors of the original logged data by 86% in data set 1, 35.1% in data set 2 and 16.6% in data set 3. On the other hand, the percentage of improvement in position errors achieved by the GPR are 23.3%, 25.7% and 16.1% for each data set respectively. These are lower in comparison with the GPR-LR-ARIMA. The LR-ARIMA models performed better than the GPR at 29.9%, 20.3% and 15.9% respectively, but their improvements were inferior compared to the GPR-LR-ARIMA.

Percentage of improvement on RMSE produced by the GPR-LR-ARIMA are 88.7%, 43.2% and 14.4% for data set 1, 2 and 3 respectively (see Figure 8). The GPR and LR-ARIMA were observed to achieve lower improvement in RMSE compared to the GPR-LR-ARIMA. The differences between the MAE and RMSE values for the GPR-LR-ARIMA in Table 6 were smaller compared to the GPR. The bigger disparity between the RMSE and MAE produced by the GPR reflects significant variance in the individual errors in the data set, which may be caused by poor model fitting. Though the GPR could improve position errors, the predicted data points are very spread out from the mean producing undesirable outliers in the model.

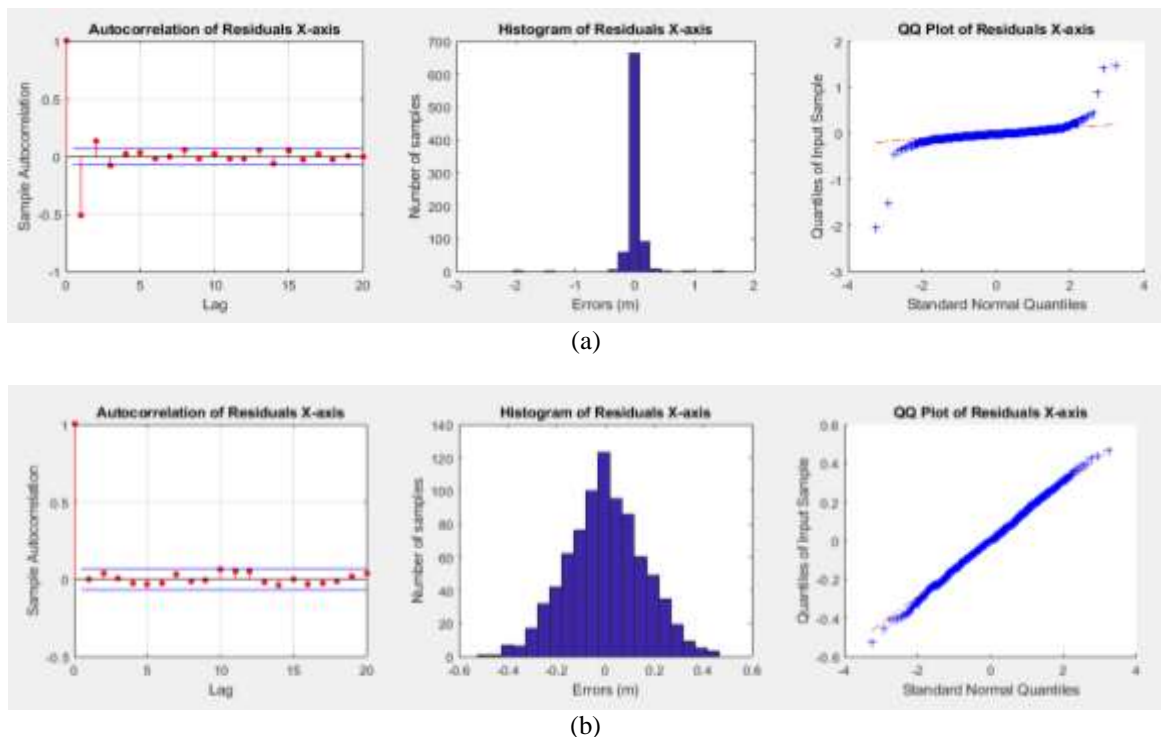
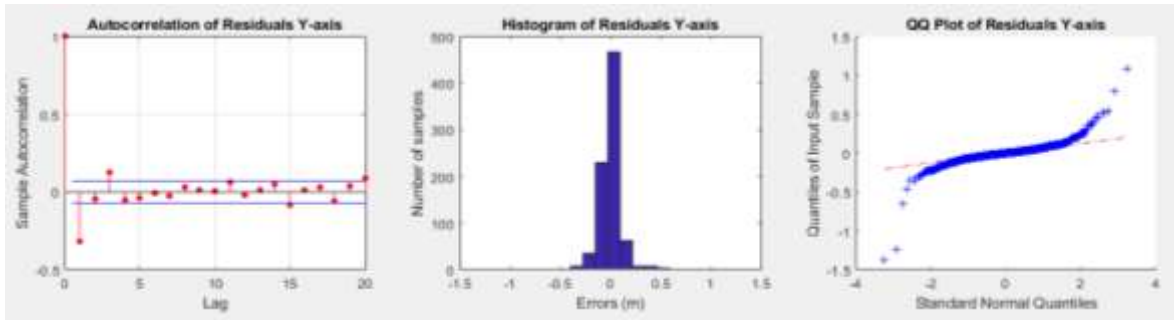
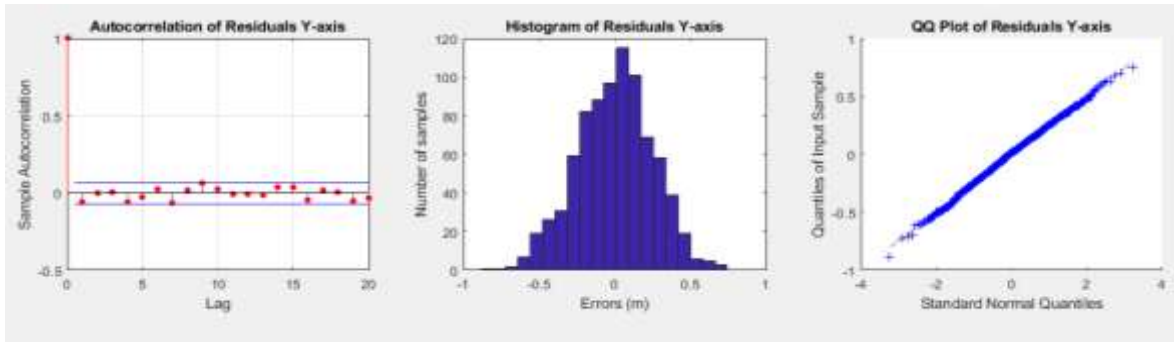


Figure 4. Comparison of model fit between sparse GPR and GPR-LR-ARIMA for x-axis of data set 2  
 (a) autocorrelation, histogram and QQ plots of sparse GPR model for x-axis of data set 2 and  
 (b) autocorrelation, histogram and QQ plots of GPR-LR-ARIMA model for x-axis of data set 2



(a)



(b)

Figure 5. Comparison of model fit between sparse GPR and GPR-LR-ARIMA for y-axis of data set 2  
 (a) autocorrelation, histogram and QQ plots of sparse GPR model for y-axis of data set 2 and  
 (b) autocorrelation, histogram and QQ plots of GPR-LR-ARIMA model for y-axis of data set 2

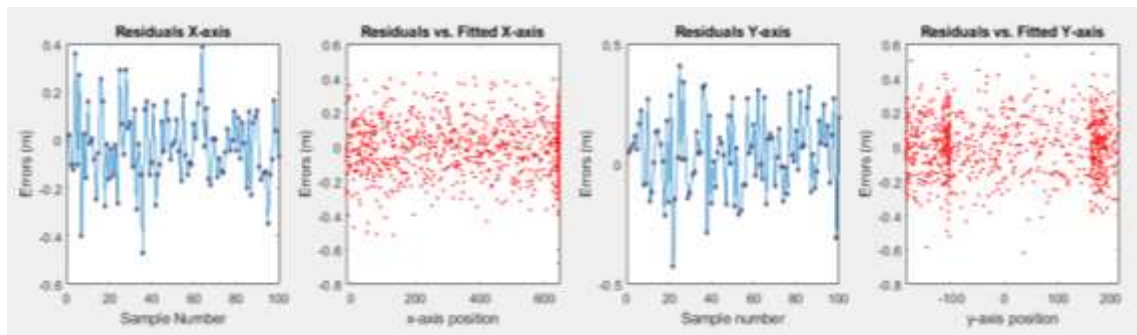


Figure 6. Scatter plots x-axis and y-axis residuals from GPR-LR-ARIMA models of data set 2

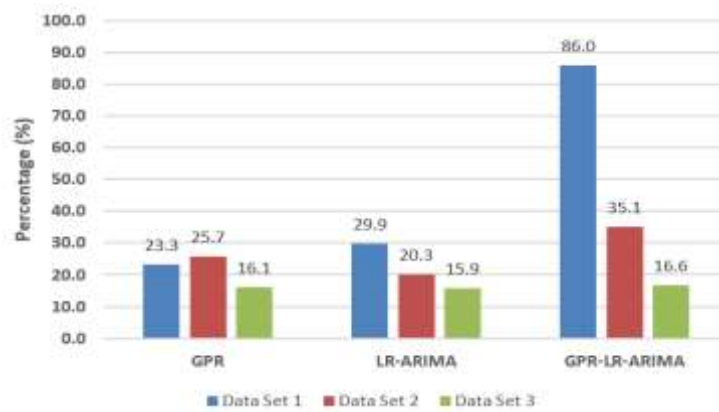


Figure 7. Percentage of improvement in 2D MAE positioning

Table 6. Comparison of 2D position errors of original data, GPR and GPR-LR-ARIMA

Data Set	Original Logged Data		GPR		LR-ARIMA		GPR-LR-ARIMA	
	MAE (m)	RMSE (m)	MAE (m)	RMSE (m)	MAE (m)	RMSE (m)	MAE (m)	RMSE (m)
1	0.4887	0.6043	0.3749	0.5017	0.3425	0.3731	<b>0.0685</b>	<b>0.0685</b>
2	0.5990	0.7642	0.4448	0.5812	0.4776	0.4776	<b>0.3888</b>	<b>0.4337</b>
3	0.5019	0.5555	0.4213	0.4884	0.4223	0.4790	<b>0.4184</b>	<b>0.4756</b>

\*bold font indicates best performance



Figure 8. Percentage of improvement in 2D RMSE positioning

#### 4. CONCLUSION

The work demonstrated the usefulness of sparse GPR to model dynamic trajectory data from RTK-GNSS that could produce improved positioning accuracy. However, evaluation on the model residuals revealed undesirable outliers that indicated poor model fit. In addition, the GPR was not able to handle correlation in the residuals signifying its inability to eliminate correlated noise. The integrated model formulation based upon the GPR-LR-ARIMA model could enhance the description and prediction of trajectory data with better model fit. The GPR-LR-ARIMA improved MAE in 2D position accuracy of the original trajectory up to 86% whereas the GPR and LR-ARIMA improved only up to 25.7% and 29.9% respectively. The integrated model displayed better model fit with normally distributed residuals; ability to eliminate correlated noise and exceptional positioning accuracy. To this end, we successfully demonstrated the drawback of the GPR can be compensated by the LR-ARIMA via the integrated approach to reduce positioning errors in localization and navigation systems.

#### ACKNOWLEDGEMENTS

This work is funded by the Malaysian Ministry of Science, Technology, and Innovation through the Technology Development Fund 1 (TDF04211376, 600-RMC/MOSTI-TeD1/5/3 (008/2021)). The authors also wish to thank College of Engineering, Universiti Teknologi MARA for supporting this project.

#### REFERENCES

- [1] R. Teguh, F. F. Adj, B. Benius, and M. Nur Aulia, "Android mobile application for wildfire reporting and monitoring," *Bulletin of Electrical Engineering and Informatics*, vol. 10, no. 6, pp. 3412–3421, 2021, doi: 10.11591/eei.v10i6.3256.
- [2] T. T. Anh, T. N. Van, and H. Le Xuan, "Developing a network time server for LEO optical tracking," *Bulletin of Electrical Engineering and Informatics*, vol. 11, no. 3, pp. 1308–1316, 2022, doi: 10.11591/eei.v11i3.3636.
- [3] A. Syetiawan, D. D. Wijaya, and I. Meilano, "Quality control in GNSS reflectometry method for tide observations," *TELKOMNIKA (Telecommunication Computing Electronics and Control)*, vol. 19, no. 6, p. 1935, 2021, doi: 10.12928/telkomnika.v19i6.21670.
- [4] P. Visconti, M. Luceri, R. Velazquez, and D. F. Roberto, "A remote-controlled global navigation satellite system based rover for accurate video-assisted cadastral surveys," *International Journal of Electrical and Computer Engineering (IJECE)*, vol. 12, no. 4, p. 3551, 2022, doi: 10.11591/ijece.v12i4.pp3551-3563.
- [5] D. S. Ilcev, "Architecture of the global navigation satellite system for maritime applications," *TELKOMNIKA (Telecommunication Computing Electronics and Control)*, vol. 18, no. 3, p. 1600, 2020, doi: 10.12928/telkomnika.v18i3.15640.
- [6] E. F. Abdelhafid, Y. M. Abdelkader, M. Ahmed, D. Rachid, and E. I. Abdelilah, "Visual and light detection and ranging-based simultaneous localization and mapping for self-driving cars," *International Journal of Electrical and Computer Engineering (IJECE)*, vol. 12, no. 6, p. 6284, 2022, doi: 10.11591/ijece.v12i6.pp6284-6292.

- [7] J. Hidalgo-Carrio, D. Hennes, J. Schwendner, and F. Kirchner, "Gaussian process estimation of odometry errors for localization and mapping," *2017 IEEE International Conference on Robotics and Automation (ICRA)*. IEEE, 2017. doi: 10.1109/icra.2017.7989670.
- [8] V. Kurtz and H. Lin, "Kalman filtering with Gaussian processes measurement noise," Sep. 2019, [Online]. Available: <http://arxiv.org/abs/1909.10582>
- [9] M. Ayaz, "Comparative study of indoor navigation systems for autonomous flight," *TELKOMNIKA (Telecommunication Computing Electronics and Control)*, vol. 16, no. 1, p. 118, 2018, doi: 10.12928/telkomnika.v16i1.6814.
- [10] F. Teng, W. Tao, and C.-M. Own, "Localization reliability improvement using deep Gaussian process regression model," *Sensors (Basel, Switzerland)*, vol. 18, no. 12, p. 4164, Nov. 2018, doi: 10.3390/s18124164.
- [11] R. Septiawan, A. Syetiawan, A. Rufiyanto, N. Taufik, B. Sulistya, and E. M. Putro, "GNSS interference reduction method for CORS site planning," *TELKOMNIKA (Telecommunication Computing Electronics and Control)*, vol. 17, no. 3, p. 1159, 2019, doi: 10.12928/telkomnika.v17i3.11744.
- [12] W. Ye, Z. Liu, C. Li, and J. Fang, "Enhanced Kalman filter using noisy input Gaussian process regression for bridging GPS outages in a POS," *Journal of Navigation*, vol. 71, no. 3, pp. 565–584, 2017, doi: 10.1017/s0373463317000819.
- [13] M. Rychlicki, Z. Kasprzyk, and A. Rosiński, "Analysis of accuracy and reliability of different types of GPS receivers," *Sensors (Basel, Switzerland)*, vol. 20, no. 22, p. 6498, Nov. 2020, doi: 10.3390/s20226498.
- [14] L. Guo, F. Wang, J. Sang, X. Lin, X. Gong, and W. Zhang, "Characteristics analysis of raw multi-GNSS measurement from Xiaomi Mi 8 and positioning performance improvement with L5/E5 frequency in an urban environment," *Remote Sensing*, vol. 12, no. 4, p. 744, 2020, doi: 10.3390/rs12040744.
- [15] T. Baybura, İ. Tiryakiöglu, M. A. Uğur, H. İ. Solak, and Ş. Şafak, "Examining the accuracy of network RTK and long base RTK methods with repetitive measurements," *Journal of Sensors*, vol. 2019, pp. 1–12, 2019, doi: 10.1155/2019/3572605.
- [16] J. Jackson, R. Saborio, S. Anas Ghazanfar, D. Gebre-Egziabher, and D. Brian, "Evaluation of low-cost, centimeter-level accuracy OEM GNSS receivers," 2018.
- [17] L. Cheng *et al.*, "An additive Gaussian process regression model for interpretable non-parametric analysis of longitudinal data," *Nature communications*, vol. 10, no. 1, p. 1798, Apr. 2019, doi: 10.1038/s41467-019-09785-8.
- [18] M. Lin *et al.*, "Robust Gaussian process regression for real-time high precision GPS signal enhancement," in *Proceedings of the 25th ACM SIGKDD International Conference on Knowledge Discovery & Data Mining*, ACM, 2019. doi: 10.1145/3292500.3330695.
- [19] T. T. Hines and E. A. Hetland, "Revealing transient strain in geodetic data with Gaussian process regression," *Geophysical Journal International*, vol. 212, no. 3, pp. 2116–2130, 2017, doi: 10.1093/gji/ggx525.
- [20] L. Kortessalmi, "Gaussian process regression-based GPS variance estimation and trajectory forecasting," Linköping University, 2018.
- [21] C. Xue-mei, W. Zi-jia, L. Meng-xi, and O. Yang-jia-xin, "A multiple-vehicle decision-making model for left-turn behavior of AVs at urban intersections based on conflict resolution," in *2020 7th International Conference on Information Science and Control Engineering (ICISCE)*, IEEE, Dec. 2020, pp. 1565–1571. doi: 10.1109/ICISCE50968.2020.00310.
- [22] Y. Yoon, C. Kim, J. Lee, and K. Yi, "Interaction-aware probabilistic trajectory prediction of cut-in vehicles using Gaussian process for proactive control of autonomous vehicles," *IEEE Access*, vol. 9, pp. 63440–63455, 2021, doi: 10.1109/access.2021.3075677.
- [23] G. Chen, W. Wang, and Y. Xue, "Identification of ship dynamics model based on sparse gaussian process regression with similarity," *Symmetry*, vol. 13, no. 10, p. 1956, 2021, doi: 10.3390/sym13101956.
- [24] J. Caldwell and J. A. Marshall, "Towards efficient learning-based model predictive control via feedback linearization and Gaussian process regression," *2021 IEEE/RSJ International Conference on Intelligent Robots and Systems (IROS)*. IEEE, 2021. doi: 10.1109/iros51168.2021.9636755.
- [25] A. Buelta, A. Olivares, E. Staffetti, W. Aftab, and L. Mihaylova, "A Gaussian process iterative learning control for aircraft trajectory tracking," *IEEE Transactions on Aerospace and Electronic Systems*, vol. 57, no. 6, pp. 3962–3973, 2021, doi: 10.1109/taes.2021.3098133.
- [26] Z. Li, P. Zhao, C. Jiang, W. Huang, and H. Liang, "A learning-based model predictive trajectory planning controller for automated driving in unstructured dynamic environments," *IEEE Transactions on Vehicular Technology*, vol. 71, no. 6, pp. 5944–5959, 2022, doi: 10.1109/tvt.2022.3159994.
- [27] Z. Zhang, B. Li, and Y. Shen, "Comparison and analysis of unmodelled errors in GPS and BeiDou signals," *Geodesy and Geodynamics*, vol. 8, no. 1, pp. 41–48, Jan. 2017, doi: 10.1016/j.geog.2016.09.005.
- [28] R. S. Nahar, K. M. Ng, F. H. K. Zaman, and J. Johari, "Modeling RTK-GNSS trajectory data using sparse gaussian process models," *2022 IEEE 18th International Colloquium on Signal Processing & Applications (CSPA)*. IEEE, 2022. doi: 10.1109/cspa55076.2022.9781923.
- [29] E. Wang, F. Yang, P. Qu, T. Pang, and X. Lan, "Weighted least squared approach to fault detection and isolation for GPS integrity monitoring," *TELKOMNIKA (Telecommunication Computing Electronics and Control)*, vol. 15, no. 3, p. 1022, 2017, doi: 10.12928/telkomnika.v15i3.5800.
- [30] K. M. Ng, R. S. Nahar, and M. IbneReaz, "Linear regression models with autoregressive integrated moving average errors for measurements from real time kinematics-global navigation satellite system during dynamic test," *International Journal of Electrical and Computer Engineering (IJECE)*, vol. 13, no. 1, p. 770, 2023, doi: 10.11591/ijece.v13i1.pp770-780.
- [31] P. Barba, B. Rosado, J. Ramírez-Zelaya, and M. Berrocoso, "Comparative analysis of statistical and analytical techniques for the study of GNSS geodetic time series," in *The 7th International conference on Time Series and Forecasting*, Basel Switzerland: MDPI, Jun. 2021, p. 21. doi: 10.3390/engproc2021005021.
- [32] R. Hohensinn, S. Häberling, and A. Geiger, "Dynamic displacements from high-rate GNSS: error modeling and vibration detection," *Measurement*, vol. 157, p. 107655, 2020, doi: 10.1016/j.measurement.2020.107655.
- [33] S. Salma, G. Sivavaraprasad, B. T. P. Madhav, and D. Venkata Ratnam, "Implementation of VARMA model for ionospheric TEC forecast over an Indian GNSS station," *2020 5th International Conference on Devices, Circuits and Systems (ICDCS)*. IEEE, 2020. doi: 10.1109/icdcs48716.2020.243568.
- [34] Z. Liu, Z. Zhu, J. Gao, and C. Xu, "Forecast methods for time series data: a survey," *IEEE Access*, vol. 9, pp. 91896–91912, 2021, doi: 10.1109/access.2021.3091162.
- [35] OpenStreetMap, "Persiaran anggerik eria." Accessed: Dec. 12, 2023. [Online]. Available: [https://www.openstreetmap.org/search?query=Persiaran Anggerik Eria#map=17/2.99536/101.52982](https://www.openstreetmap.org/search?query=Persiaran+Anggerik+Eria#map=17/2.99536/101.52982)

## BIOGRAPHIES OF AUTHORS



**Ravenny Sandin Nahar**     graduated with Bachelor of Engineering (Hons.) Electronic Engineering at the Faculty of Electrical Engineering, Universiti Teknologi Mara (UiTM) in 2019. He has also completed his post graduate studies in Master in Engineering (Electrical Engineering) at the School of Engineering, College of Engineering, Universiti Teknologi MARA, Shah Alam. His research interest includes artificial intelligence and smart systems. He can be contacted at email: ravenhiccup297@gmail.com.



**Kok Mun Ng**     received the B.Eng (Hons) and M.Eng degrees in systems engineering from the Universiti Tun Hussein Onn, Malaysia, in 2002 and 2006 respectively. He obtained the Ph.D. degree in Systems Engineering from Universiti Kebangsaan Malaysia, Bangi, Malaysia in 2016. From 2002 to 2003, he worked as a system engineer at Matromatics Handling Systems, Malaysia. He was with Stamford College, Malaysia from 2006 to 2008 as a lecturer before joining the School of Electrical Engineering, Universiti Teknologi MARA, where he works as a senior lecturer at the Systems Engineering department. His research interests include system modeling and optimization, artificial intelligence, intelligent transportation systems, mapping and localization. He is a sub-editor of the Journal of Electrical & Electronic Systems Research (JEESR) and a research fellow at the university vehicle telematics industrial research lab. He can be contacted at email: ngkokmun@uitm.edu.my.



**Fadhlhan Hafizhelmi Kamaru Zaman**     received the B.Sc (Hons.) and P.h.D. degrees from International Islamic University Malaysia in 2008 and 2015, respectively. He is currently an Associate Professor at the College of Engineering, Universiti Teknologi MARA, Malaysia. His research interests are in surveillance systems, pattern recognition, signal and image processing, artificial intelligence, and computer vision. He is also the Head of the Vehicle Intelligence and Telematics Lab. Fadhlhan is also a professional Engineer with the Board of Engineers Malaysia, and a Chartered Engineer from the Institution of Engineering and Technology, UK. He can be contacted at email: fadhlhan@uitm.edu.my.



**Noorfadzli Abdul Razak**     completed his Ph.D. in Electrical Engineering at Universiti Teknologi MARA (UiTM) in 2019. He received his Master of Electrical Engineering from Universiti Teknologi Malaysia (UTM) in 2017. In 2004, he obtained a Bachelor of Electrical Engineering from Kolej Universiti Teknologi Tun Hussein Onn (KUiTTHO). He started his carrier as a Vocational Training Officer in Kolej Kemahiran Tinggi MARA, Balik Pulau from 2005 to 2008. He then joined the School of Electrical Engineering, College of Engineering, UiTM, Shah Alam, Selangor as a lecturer from 2009 until today. Currently, he heads the Innovative Electromobility (ITEM) Research Lab. He actively conducts research and development along with publishing journals and papers in autonomous control, mobile robot, and automation system. All his works in these areas are supported with many grants either locally or internationally. He actively does consultancies and training for industries and educational institutions. He is also a Certified Energy Manager (CEM-GreenTech) and Certified Human Resources Development Fund (HRDF-MIDA). He can be contacted at email: noorfadzli@uitm.edu.my.



**Juliana Johari**     received Ph.D. in Micro-Engineering and Nano-Electronics from Universiti Kebangsaan Malaysia, Master degree in Biomedical Engineering from University of Surrey, United Kingdom and Bachelor in Electrical and Electronics Engineering from University of Strathclyde, United Kingdom. She is currently an Associate Professor in Control System and Instrumentation Engineering at the School of Electrical Engineering, Universiti Teknologi MARA Malaysia and Affiliate Professor in Electronics and Instrumentation Engineering at the B.S. Abdur Rahman Crescent Institute of Science and Technology, Chennai, India. Area of specialization including robotics, automation, MEMS and Artificial Intelligence. She can be contacted at email: julia893@uitm.edu.my.